

Structure-Texture Decomposition of Images with Interval Gradient

Hyunjoon Lee¹, Junho Jeon¹, Junho Kim² and Seungyong Lee¹

¹POSTECH, Pohang, Korea
 {crowlove, zwitterion27, leesy}@postech.ac.kr
²Kookmin University, Seoul, Korea
 junho@kookmin.ac.kr

Abstract

This paper presents a novel filtering-based method for decomposing an image into structures and textures. Unlike previous filtering algorithms, our method adaptively smooths image gradients to filter out textures from images. A new gradient operator, the interval gradient, is proposed for adaptive gradient smoothing. Using interval gradients, textures can be distinguished from structure edges and smoothly varying shadings. We also propose an effective gradient-guided algorithm to produce high-quality image filtering results from filtered gradients. Our method avoids gradient reversal in the filtering results and preserves sharp features better than existing filtering approaches, while retaining simplicity and highly parallel implementation. The proposed method can be utilized for various applications that require accurate structure-texture decomposition of images.

Keywords: texture filtering, interval gradient, gradient-domain image decomposition, 1D filtering

ACM CCS: I.4.3 [Image Processing and Computer Vision]: Enhancement–Smoothing; I.3.7 [Computer Graphics]: Three-Dimensional Graphics and Realism—Colour, shading, shadowing, and texture

1. Introduction

In structure-texture decomposition, an image is decomposed as $I = S + T$, where I , S and T represent the input image, structure elements and texture details, respectively. In general, the structure-texture decomposition problem is formulated as finding an appropriate (or latent) structure S by suppressing texture details T in the input image I . Due to its usefulness in a broad range of image processing applications, several methods have been proposed to handle this problem, which in general can be divided into two categories: optimization-based [ROF92, Wei06, XLXJ11, XYXJ12, HBZW14] and filtering-based approaches [PHK11, KEE13, CLKL14, ZSXJ14].

Optimization-based approaches [ROF92, XLXJ11, XYXJ12, HBZW14] globally suppress the oscillating patterns induced from T , while guessing the structure image S as similar as possible to the input image I . Although they obtain high-quality results, these methods are comparably complex and cannot easily be parallelized, thus not allowing the algorithm to handle large images and used in interactive applications. Filtering-based algorithms [KEE13, CLKL14, ZSXJ14] try to design effective filter kernels to suppress T . Previous

filtering approaches, however, often fail to accurately detect S for structure edges and corners.

In this paper, we propose a novel filtering-based method for structure-texture decomposition that generates high-quality results comparable to those of optimization-based approaches. Unlike most previous filtering-based approaches, we formulate the problem as $\nabla I = \nabla S + \nabla T$ in the gradient domain. Our approach directly manipulates gradients of the input image to filter out textures from the input. In this sense, our goal is to carefully design a gradient domain solution for structure-texture decomposition, where the desirable ingredients are (i) structure-aware gradient smoothing, which suppresses ∇T while preserving ∇S , and (ii) reconstruction of the filtered image from the smoothed gradients, which not only preserves ∇S but also reflects the overall shape of the input I .

Our contribution is two-fold. First, we define a new type of gradient operator, called the *interval gradient*, denoted by $\nabla_\Omega(\cdot)$, which is designed to distinguish ∇T from ∇S in the spatial support Ω . We propose a gradient rescaling method based on the interval gradient to suppress ∇T while preserving ∇S within the signal (Section 3).

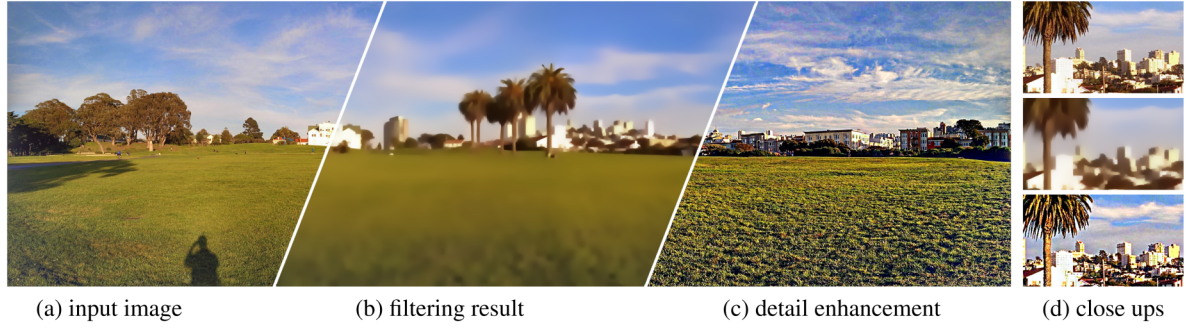


Figure 1: Structure-texture decomposition result. From the input image (a), textures are first filtered (b) and then enhanced (c). Our filtering result precisely preserves structure edges, and no artefact is introduced during the enhancement, as shown in (d).

Second, motivated by the guided image filter [HST10], we propose a novel gradient-based image filtering method that is suitable for structure-texture decomposition (Section 4). It inherits the characteristics of the guided image filter. The filtering results resemble the input images and at the same time preserve strong edges and gradients precisely, while detailed textures and repeated patterns are removed. In addition, the proposed method is composed of 1D local filters, similarly to [GO11], allowing extreme acceleration with modern GPUs. As a result, our method can decompose textures from images effectively and accurately, allowing the decomposed images to be utilized in various applications that require high-quality decomposition results, as shown in Figure 1.

2. Related Work

2.1. Structure-texture image decomposition

Among the filtering-based approaches, the bilateral filter [TM98] is a representative kernel-based edge-preserving filter. Its range weight function allows data point pairs across edges to be clearly distinguished and thus not mixed. The guided filter [HST10] performs local linear transforms of a guidance image, a strategy that does not lead to gradient distortions near edges. The domain transform method [GO11] delivers a significant speedup in two-dimensional (2D) filtering by reducing the dimensionality to one. These methods can produce high-quality edge-preserving smoothing results but cannot easily remove strong textures.

Several methods have been proposed for removing strong textures within images. Subr *et al.* [SSD09] computed envelopes defined from local extrema and smoothed out texture oscillations by averaging the envelopes. The histogram filter [KS10], median filter [Wei06, MHW*13, ZXJ14] and diffusion-based approaches [Wei98, VPS03] are capable of filtering textures to some extent, unless the textures contain large oscillating signals. Karacan *et al.* [KEE13] proposed a patch-based texture removal algorithm that uses similarity measures based on regional covariance. The bilateral texture filter [CLKL14] uses joint bilateral filtering with a guidance image generated via a patch shift mechanism. The rolling guidance filter (RGF) [ZSXJ14] uses a Gaussian-blurred image as a guidance image in joint bilateral filtering to eliminate only the image structures that are smaller than a specific scale.

The total variation (TV) method [ROF92] effectively suppresses textures of arbitrary shapes by enforcing TV regularization constraints on the image. The weighted least squares (WLS) method [FFLS08] solves a large linear system to provide progressive/multi-scale image coarsening and decomposition. L_0 gradient minimization [XLXJ11] globally optimizes the quality of filtering by controlling the number of non-zero gradients in the image. Xu *et al.* [XYXJ12] introduced relative total variation (RTV) which allows accurate identification and removal of texture regions. As compared to filtering-based approaches, optimization-based techniques [FFLS08, XLXJ11] are able to produce high-quality results; however, their computation costs are higher in general, even when the multi-grid method [BFGS03, GWL*03] or a fast global solver based on separable application of a sequence of 1D subsystems [MCL*14] is applied.

2.2. Gradient domain image processing

Gradient domain analysis has been successfully utilized in various image processing applications, such as editing, composition, High dynamic range (HDR) image compression [FLW02, PGB03, Aga07, FHL*09, BZCC10]. We refer the reader to an excellent tutorial [AR07] for details. From an input image, the gradient information of each pixel is first computed by measuring intensity differences between the pixel and its neighbourhood. Then, these gradients are manipulated according to application-specific purposes, while their local structures are preserved. The resultant image is then estimated based on the manipulated gradients through optimization, for example, using the Poisson solver. Our local filtering approach is based on gradient domain processing specifically designed to handle the structure-texture decomposition problem.

Our approach has a connection to Retinex-based approaches for intrinsic image decomposition [TFA05, GJAF09, BST*14], in that both consider gradient-domain image decomposition. In the Retinex theory [LM71], an image could be decomposed into illumination and reflectance parts in the log-scale gradient domain, based on the assumption that illumination varies gradually but reflectance does abruptly. Retinex-based approaches use trained classifiers [TFA05] or global optimization [BST*14] to achieve illumination-reflectance decomposition in the gradient domain. Our approach tackles structure-texture decomposition in the gradient domain by defining interval gradients to handle complicated texture patterns.

3. Interval Gradient for Gradient Filtering

In structure-texture decomposition, an input image is decomposed into a structure image and a texture image. The structure part contains non-repeating edges and smooth shadings, while the texture part contains oscillating patterns and noise. The goal of the texture filtering is to find a structure image as similar as possible to the input image while removing textures. In this section, we first define the local characteristics of structure and texture in the 1D domain. Then we present our interval gradient operator, which is able to distinguish structure and texture from a given 1D signal.

3.1. Structure and texture in one dimension

In a 1D signal I , for a local window Ω_p centred at a pixel p , we define structure S as non-repeating salient edges that are smoothly increasing or decreasing signals within the window. Texture T is then defined as local oscillations added to the structure so that $I = S + T$.

Given the definition of a structure, we define that Ω_p is texture-free if and only if the signal is only increasing or decreasing but never oscillates within Ω_p . The signal can vary smoothly (smooth shading) or abruptly (structure edge). Although imperfect (e.g. the signal can smoothly go up and then down without containing texture), this definition is effective in most cases. We can then determine whether a 1D signal I is texture-free by computing a measure based on this definition. Note that the RTV metric defined in [XYXJ12] is also minimized when the signal is increasing or decreasing. In this paper, we present a novel operator, the interval gradient, to determine whether a signal is texture-free.

3.2. Definition of interval gradient

In a 1D discrete signal I , for a pixel p , one common gradient operator is the forward differentiation, defined as

$$(\nabla I)_p = I_{p+1} - I_p. \quad (1)$$

It measures the difference between two adjacent signal values. In contrast, our interval gradient for pixel p is defined as

$$(\nabla_\Omega I)_p = g_\sigma^r(I_p) - g_\sigma^l(I_p), \quad (2)$$

where g_σ^r and g_σ^l , respectively, represent left and right clipped 1D Gaussian filter functions defined by

$$\begin{aligned} g_\sigma^r(I_p) &= \frac{1}{k_r} \sum_{n \in \Omega(p)} w_\sigma(n - p - 1) I_n, \\ g_\sigma^l(I_p) &= \frac{1}{k_l} \sum_{n \in \Omega(p)} w_\sigma(p - n) I_n. \end{aligned} \quad (3)$$

w_σ is the clipped exponential weighting function with a scale parameter σ :

$$w_\sigma(x) = \begin{cases} \exp\left(-\frac{x^2}{2\sigma^2}\right) & \text{if } x \geq 0 \\ 0 & \text{otherwise} \end{cases}, \quad (4)$$

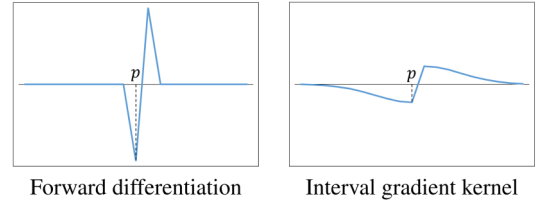


Figure 2: Forward differentiation and interval gradient kernels. Left: Conventional forward difference kernel; right: our interval gradient kernel with $\sigma = 3$.

and k_r and k_l are normalizing coefficients defined as

$$k_r = \sum_{n \in \Omega(p)} w_\sigma(n - p - 1) \text{ and } k_l = \sum_{n \in \Omega(p)} w_\sigma(p - n). \quad (5)$$

The kernel shape of the interval gradient is shown in Figure 2.

Unlike forward differentiation, the interval gradient measures the difference between the weighted averages of the left and right parts of the signal around a pixel. It is also different from gradients of the smoothed signal, as discussed in Section 3.3.

For the shape of the interval gradient kernel, any type of kernel, such as concatenation of two box filters or derivatives of Gaussian, can be used if it is able to detect the average statistics of the left and right subregions of a pixel. Different kernels have different properties when smoothing textures, as discussed in Section 5. Our experiments showed that the proposed kernel shape in Equation (4) preserves sharp features while smoothing textures. It is used to generate all examples in this paper unless otherwise stated.

3.3. Characteristics of interval gradient

The most important characteristic of the interval gradient is that for a local window Ω_p , $|(\nabla I)_p| \leq |(\nabla_\Omega I)_p|$ if the window is texture-free. As defined in Section 3.1, Ω_p is texture-free if the signal is increasing or decreasing. For the increasing case, $I_{p+1} \leq g_\sigma^r(I_p)$ and $I_p \geq g_\sigma^l(I_p)$, making the above inequality true, and similar argument holds for the decreasing case. In addition, the sign of $(\nabla_\Omega I)_p$ captures the overall increasing/decreasing tendency of the signal within Ω_p .

These characteristics can also be shown by considering the interval gradient kernel in the gradient domain. We can show that a symmetric interval gradient kernel is equivalent to an unnormalized smoothing kernel in the gradient domain, where the sum of the kernel weights is greater than 1 (see the Appendix). For a structure element p , $(\nabla_\Omega I)_p$ becomes bigger than $(\nabla I)_p$, since the smoothing kernel magnifies the gradient. For a texture region, $(\nabla_\Omega I)_p$ becomes smaller than $(\nabla I)_p$ as oscillating gradients with different signs cancel each other. The sign of $(\nabla_\Omega I)_p$ is the same as that of the weighted average of gradients, since scaling does not affect the sign.

Case by case analysis. Four example cases are shown in Figure 3. For a local window with texture, oscillations are cancelled out because of the smoothing operators g_σ^r and g_σ^l , and $|(\nabla_\Omega I)_p|$ becomes much smaller than $|(\nabla I)_p|$. For a strong structure edge,

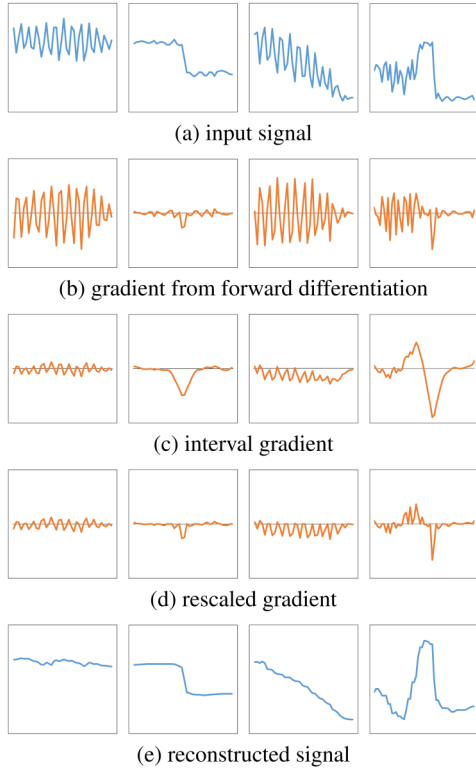


Figure 3: Various types of signals and gradients. From left to right: texture, structure edge, texture with shading and noisy valley near a structure edge.

the shape of interval gradients resembles that of the gradient of the smoothed edge. For a local window mixed with shading and textures, the magnitudes of interval gradients are smaller than those of pixel gradients but their signs indicate the overall increasing/decreasing tendency of the signal within the window. The rightmost column shows a noisy valley attached to a structure edge. In the noisy valley, similar to a mixture of shading and texture, $|(\nabla_\Omega I)_p|$ is smaller than $|(\nabla I)_p|$, although the sign of $|(\nabla_\Omega I)_p|$ changes with overall shape of the valley. However, as the signal moves into the structure edge, the magnitudes of interval gradients increase and become larger than those of pixel gradients.

Validation. To validate the property of our interval gradient, we conducted the following experiment. We filtered 200 images in the dataset given in [XYXJ12], using previous texture filtering methods [XYXJ12, ZSXJ14, CLKL14]. Then, we measured the ratios between the magnitudes of the original and interval gradients ($|(\nabla_\Omega I)_p/(\nabla I)_p|$) for all pixels in the two images, before and after filtering. As shown in Figure 4, most ratio values are near to or greater than 1 for the filtered images, while the original images have many small ratio values because of high contrast textures and noise.

Using interval gradients we can determine whether a local window of a given signal contains texture. In addition, we can determine the overall increasing/decreasing tendency of the signal. We present our gradient rescaling algorithm based on these characteristics in the following subsection.

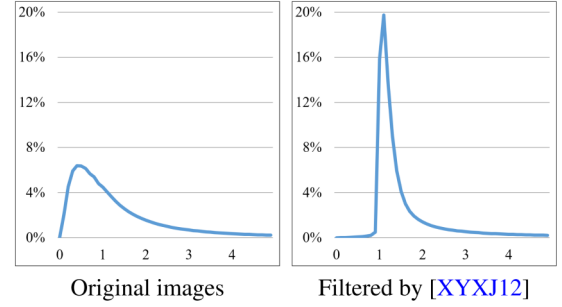


Figure 4: (x-axis) gradient ratio, $|(\nabla_\Omega I)_p/(\nabla I)_p|$; (y-axis) percentage of pixels. The total number of pixels is around 100 M. The image gradients along the horizontal direction were used for the comparison, and the result with the vertical gradients is similar. After texture filtering, almost all pixels have gradient ratios near to or greater than 1.

3.4. Gradient rescaling with interval gradients

In order to produce a texture-free signal from an input signal I , the gradients within texture regions should be suppressed. Furthermore, the signal should be either increasing or decreasing for all local windows Ω_p . With these objectives, we use the following equation to rescale the gradients of the input signal with the corresponding interval gradients:

$$(\nabla' I)_p = \begin{cases} (\nabla I)_p \cdot w_p & \text{if } \text{sign}((\nabla I)_p) = \text{sign}((\nabla_\Omega I)_p) \\ 0 & \text{otherwise,} \end{cases} \quad (6)$$

where $(\nabla' I)_p$ represents the rescaled gradient, and w_p is the rescaling weight:

$$w_p = \min \left(1, \frac{|(\nabla_\Omega I)_p| + \epsilon_s}{|(\nabla I)_p| + \epsilon_s} \right), \quad (7)$$

where ϵ_s is a small constant to prevent numerical instability. Too small values of ϵ_s would make the algorithm sensitive to noise, introducing unwanted artefacts to filtering results. The sensitivity to noise can be reduced by increasing ϵ_s but textures could not be completely filtered if ϵ_s is too big. We set $\epsilon_s = 10^{-4}$ in our implementation.

For structure edges and smoothly varying regions, gradients are not changed because $|(\nabla_\Omega I)_p| \geq |(\nabla I)_p|$, making w_p be 1. On the other hand, for textured regions with oscillating patterns and noise, $|(\nabla_\Omega I)_p| < |(\nabla I)_p|$ and the gradients are suppressed with w_p less than 1. In addition, $(\nabla I)_p$ is set to zero if the signs of the original and interval gradients are different. As our goal is to make a signal locally monotonic, we make $(\nabla I)_p$ follow the local increasing/decreasing tendency, which is estimated by the sign of $(\nabla_\Omega I)_p$, by setting $(\nabla I)_p$ to zero if it does not agree with the tendency.

As a result, the filtered gradients satisfy the first property specified in Section 1, preserving ∇S and suppressing ∇T . However, the textures may not be fully filtered for some regions, and stair-like effect can occur within a region containing both texture and smoothly

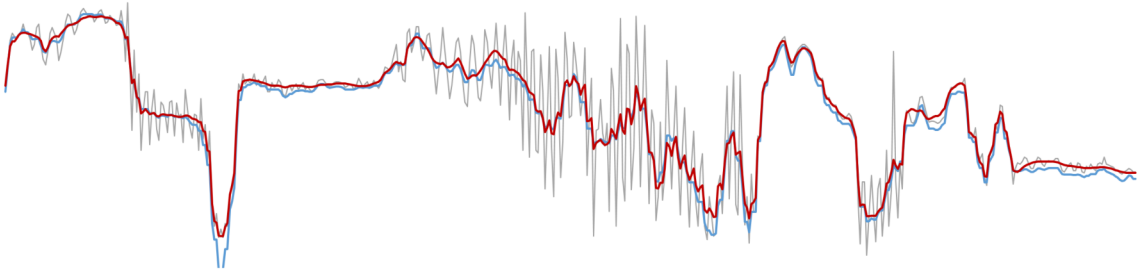


Figure 5: Gradient-based guided filtering example: (grey) input signal; (blue) signal reconstructed directly from rescaled gradients; (red) signal after guided filtering. In the right part of the signal, the directly reconstructed signal becomes deviated from the original. This deviation error is adjusted by using the guided filtering, as shown by the red curve.

varying shading, as shown in Figure 3e. These remaining issues are handled in the following section.

4. Texture Filtering with Interval Gradient

4.1. 1D texture filtering

After gradient rescaling, we can reconstruct the filtered signal by simply accumulating the rescaled gradients. The accumulation result, however, can still contain small unfiltered oscillations and deviate from the original signal, since we have rescaled gradients locally (Figures 3e and 5). We need a method for rectifying the reconstructed signal to remove remaining oscillations and to remedy the deviations from the original signal. Guided filtering [HST10] provides an appropriate solution for this task, as it filters the input signal to remove small noise and match the target signal. Guided filtering is also known to preserve edges and corners without introducing gradient distortions and oversharpened edges.

To obtain the filtering result of the input signal I , we first construct a temporary signal R from the rescaled gradients via accumulation:

$$R_p = \sum_{k=0}^{p-1} I_0 + (\nabla' I)_k, p \in \{0, 1, \dots, N_p\}, \quad (8)$$

where I_0 is the leftmost value of I and N_p is the number of pixels in I . Then, for each reconstructed signal value R_p , the 1D guided filtering process seeks the best linear transform coefficients a_p and b_p that minimize:

$$\arg \min_{a_p, b_p} \sum_{n \in N(p)} w_n \left((a_p R_n + b_p - I_n)^2 + \epsilon a_p^2 \right), \quad (9)$$

where w_n is the Gaussian weight with the scale parameter σ in Equation (4), given as

$$w_n = \exp \left(-\frac{(n-p)^2}{2\sigma^2} \right), \quad (10)$$

and ϵ is the smoothness parameter. The effects of the parameters σ and ϵ are discussed in Section 5. Closed form solutions exist for

both a_p and b_p , as given in [HST10]:

$$a_p = \frac{g_\sigma((RI)_p) - g_\sigma(R_p)g_\sigma(I_p)}{g_\sigma(R_p^2) - g_\sigma(R_p)^2 + \epsilon}, \quad (11)$$

$$b_p = g_\sigma(I_p) - a_p \cdot g_\sigma(R_p), \quad (12)$$

where $g_\sigma(\cdot)$ represents 1D Gaussian smoothing with σ and RI is the elementwise multiplication of R and I . Then the filtered result S can be computed as

$$S_p = \bar{a}_p R_p + \bar{b}_p, \quad (13)$$

where $\bar{a}_p = g_\sigma(a_p)$ and $\bar{b}_p = g_\sigma(b_p)$ are Gaussian smoothed coefficients. Figure 5 shows an example of the guided filtering process; structural differences from the original as well as the remaining oscillations in the temporary signal are removed in the filtering.

Algorithm 1 2D image filtering

Input: image I

Output: texture filtered image S

while Eq. (14) is false **do**

$(\nabla'_x I) \leftarrow$ rescaled gradients along x-axis \triangleright Eq. (6)

$(\nabla'_y I) \leftarrow$ rescaled gradients along y-axis

for $i := 0 \dots (N_d - 1)$ **do**

$\sigma_i \leftarrow \sigma \cdot \sqrt{3} \frac{2^{N_d-i}}{\sqrt{4^{N_d}-1}}$ \triangleright Adapted from [GO11]

$S_x \leftarrow$ 1D filtering result along x-axis

\triangleright Eqs. (11)-(13)

$I \leftarrow S_x$

$S_y \leftarrow$ 1D filtering result along y-axis

$I \leftarrow S_y$

end for

end while

$S \leftarrow I$

4.2. 2D texture filtering

So far, all the algorithm components, the interval gradient, gradient rescaling and guided filtering, have been defined and applied in the

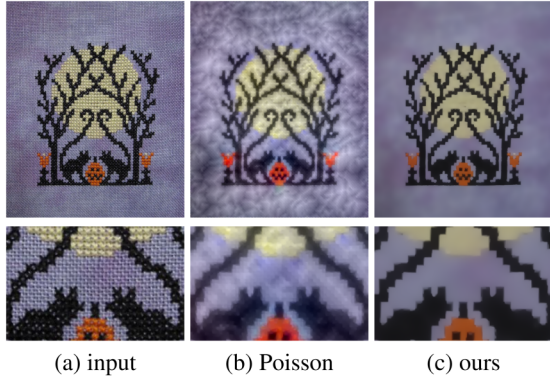


Figure 6: Comparison between Poisson reconstruction and our approach. Due to remaining oscillations in the filtered gradients, Poisson reconstruction generates an unpleasing result. With our guided filtering, such remaining oscillations are filtered out while structure edges are preserved.

1D domain. To apply these components to a 2D image, we adopt the approach of alternating 1D filtering operations in the x and y directions, which was used for domain transform filtering [GO11]. We first compute the rescaled gradients in both x and y directions from the input image. At each iteration, we apply 1D filtering to the image along the x direction using Equations (11)–(13). The filtered result is then set as the input and the 1D filtering along the y direction is applied with the rescaled gradients computed at the beginning. As in domain transform filtering [GO11], these alternating steps are performed several times with decreasing spatial support σ_i . By taking only 1D operations, our 2D filtering can be performed efficiently.

A possible alternative approach to handle 2D images using our algorithm components would be to compute filtered gradients in the x and y directions using interval gradient and gradient rescaling, and then apply the Poisson reconstruction method [PGB03] to the filtered gradients. However, as shown in Figure 6, such an approach is not very successful in our case, as the Poisson solver usually fails in the presence of noise and outliers, often producing over-smoothed results [AR07]. Remaining small oscillations from textures in the filtered gradients act as noise that does not favour a desirable output image, and a Poisson solver could return the texture patterns into the output. Moreover, the over-smoothing artefact of a Poisson solver blurs structural boundaries in the output.

Filtering iterations. Iterative filtering is necessary to fully remove high contrast textures from images [CLKL14]. To obtain the final result, the entire process, consisting of interval gradient computation, gradient smoothing and iterative 1D filtering, is repeated several times, where the result obtained from the previous iteration is used as the input of the current iteration. For a stopping condition, we check whether the filtering iteration has been converged. As textures are removed, interval gradients become bigger, and the rescaling ratio in Equation (7) becomes 1 for most pixels. Utilizing this, we measure the difference of rescaling ratios between the current and

previous iterations. The iteration is stopped when the difference is less than a given threshold δ_t , so that

$$\max \left(\frac{1}{N} \sum_p \left(w_{px}^{t-1} - w_{px}^t \right)^2, \frac{1}{N} \sum_p \left(w_{py}^{t-1} - w_{py}^t \right)^2 \right) < \delta_t, \quad (14)$$

where w_{px}^t and w_{py}^t are the rescaling ratios for the x - and y -directional gradients of a pixel p at iteration t , respectively. Algorithm 1 summarizes the entire process of our 2D filtering method.

5. Experimental Results

Parameters. As in previous structure-preserving filtering methods, our method has two main control parameters, σ and ϵ . Parameter σ controls the scale of textures to be removed, and ϵ controls the smoothness of the result. In our experiments, we used $\sigma \in [2, 5]$ and $\epsilon \in [0.01^2, 0.03^2]$. Figure 7 shows filtering examples to demonstrate the effects of the parameters. For the convergence threshold δ_t in Equation (14), too small values would bring in unnecessary filtering iterations and oversmooth the image, while bigger values could cause the filtering process to stop too early. We used a fixed value of 0.05^2 throughout our experiments. We found that more iterations (usually 5–8) are required to filter high contrast textures, while 3–5 iterations suffice for most cases.

Interval gradient kernel shapes. Various kernels can be applied to compute interval gradients provided that they capture the signal difference between the two intervals in the left and right of a pixel. We tested three different kernels, clipped Gaussian, box shaped and derivative of Gaussian (DoG) (Figure 15). In principle, sharp features such as corners are preserved better if more weights are given near to the kernel centre. On the other hand, high contrast textures can be effectively removed using the DoG kernel (Figure 8). Results with the box-shaped kernel show slightly inferior quality, but can be efficiently computed with integral images. In our experiments, we used clipped Gaussian kernels for most images, unless stated otherwise.

Handling colour images. For filtering colour images, we use the gradient sums of colour channels in the gradient rescaling step (Equations (6) and (7)), that is,

$$w_p = \min \left(1, \frac{\sum_{c \in \{r,g,b\}} |(\nabla_\Omega I^c)_p| + \epsilon_s}{\sum_{c \in \{r,g,b\}} |(\nabla I^c)_p| + \epsilon_s} \right). \quad (15)$$

In the guided filtering process, the colour bleeding artefact may occur if each channel is filtered independently. Guided filtering for colour images is described in [HST10]; however, it requires a 3-by-3 matrix inversion for each pixel and that the target image be single channel. Instead, we use a simple approach to prevent the colour bleeding artefact. Colour bleeding happens when a_p in Equation (11) of a specific colour channel becomes very small as compared to those of the other channels during the filtering. In this case, the

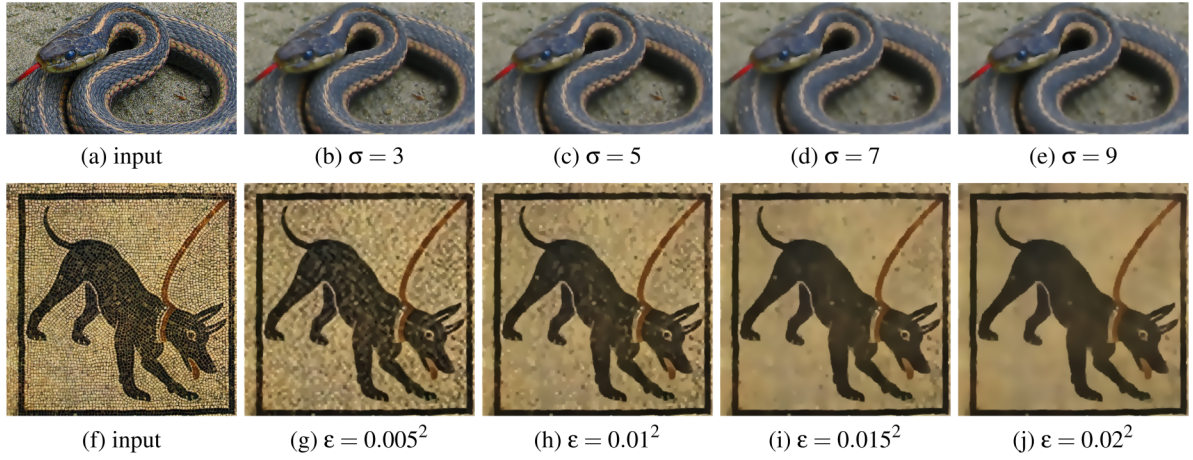


Figure 7: Results with varying parameters: (top) bigger scale textures are removed as σ increases; (bottom) smoother results are obtained with bigger ϵ .

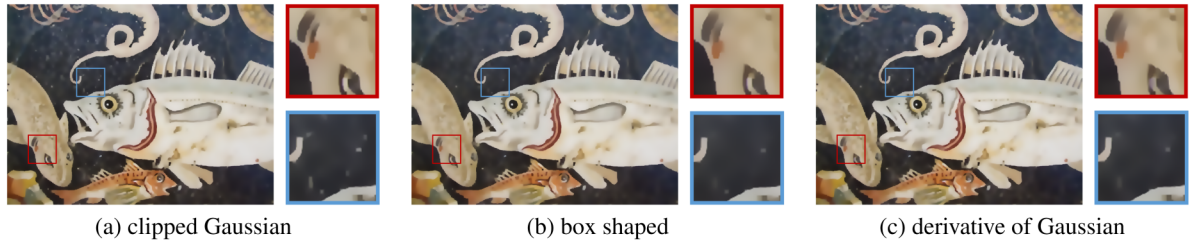


Figure 8: Results using three different interval gradient kernels. The clipped Gaussian kernel preserves sharp features better, while the derivative of Gaussian kernel is able to effectively smooth high contrast textures. A box shaped kernel smooths textures moderately. All the parameters, except for the interval gradient kernel shape, are set the same for the three cases.

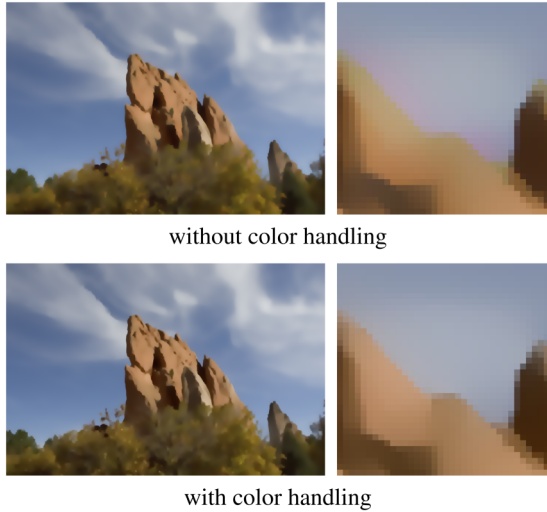


Figure 9: Colour handling example. In the top row, guided filtering is applied separately for each channel, and the red colour channel is over-smoothed, causing colour bleeding. Colour bleeding can be prevented using Equations (16) and (17), as shown in the bottom row.

colour channel is blurred while other channels are not. To prevent this, for each pixel we compute the minimum threshold of a_p as

$$a_p^{max} = \min \left(1, \max_{c \in \{r, g, b\}} a_p^c \right), \quad (16)$$

where a_p^c represents the scaling factor for a colour channel c . The value of a_p^{max} is clamped by 1 to avoid unnecessary scale-up of a channel value. Then, we adjust a_p^c of each colour channel using the threshold a_p^{max} as

$$a_p^c = \max (a_p^c, a_p^{max}). \quad (17)$$

Figure 9 shows an example of colour handling.

Timing data. Table 1 shows the average computation time. Although our method is not significantly faster than previous approaches when running on a CPU, it is highly parallelizable because of its local nature. In addition, our method consists only of 1D filters, allowing the fast shared memory structure of CUDA to be used [NBGS08]. Our implementation using CUDA C++ can run around 400 times faster than the CPU version.

Table 1: Timing data for a greyscale image of 600×800 pixels with a single filtering iteration, measured using our MATLAB (CPU) and CUDA C++ (GPU) implementations on a PC with Intel Core i7 CPU, 12 GB RAM and NVIDIA GeForce GTX 980 graphic card running Windows 8.1.

Component	$\sigma = 3$ CPU/GPU	$\sigma = 5$ CPU/GPU	$\sigma = 7$ CPU/GPU
Comp. $(\nabla' I)$	80 ms/0.6 ms	90 ms/1 ms	95 ms/1.5 ms
Comp. S	390 ms/7.5 ms	530 ms/11 ms	545 ms/15 ms
Total	470 ms/8.1 ms	620 ms/12 ms	640 ms/16.5 ms

Comparison. We compared our filtering method with a few previous approaches [XYXJ12, CLKL14, ZSXJ14]. For RTV [XYXJ12] and RGF [ZSXJ14], we used the authors’ implementations publicly available on internet. For bilateral texture filtering (BTF) [CLKL14], we used our own implementation. Figure 10 shows comparison examples. Similar to other methods, our method preserves the structure

elements while textures are filtered out. Compared to BTF and RGF, our method preserves small features and edge gradients better. Our results show comparable quality to those of RTV with significantly less processing time, as shown in Table 1. As an optimization-based method, RTV flattens shading variations in the input image, and shading information can be lost in the filtering results although they

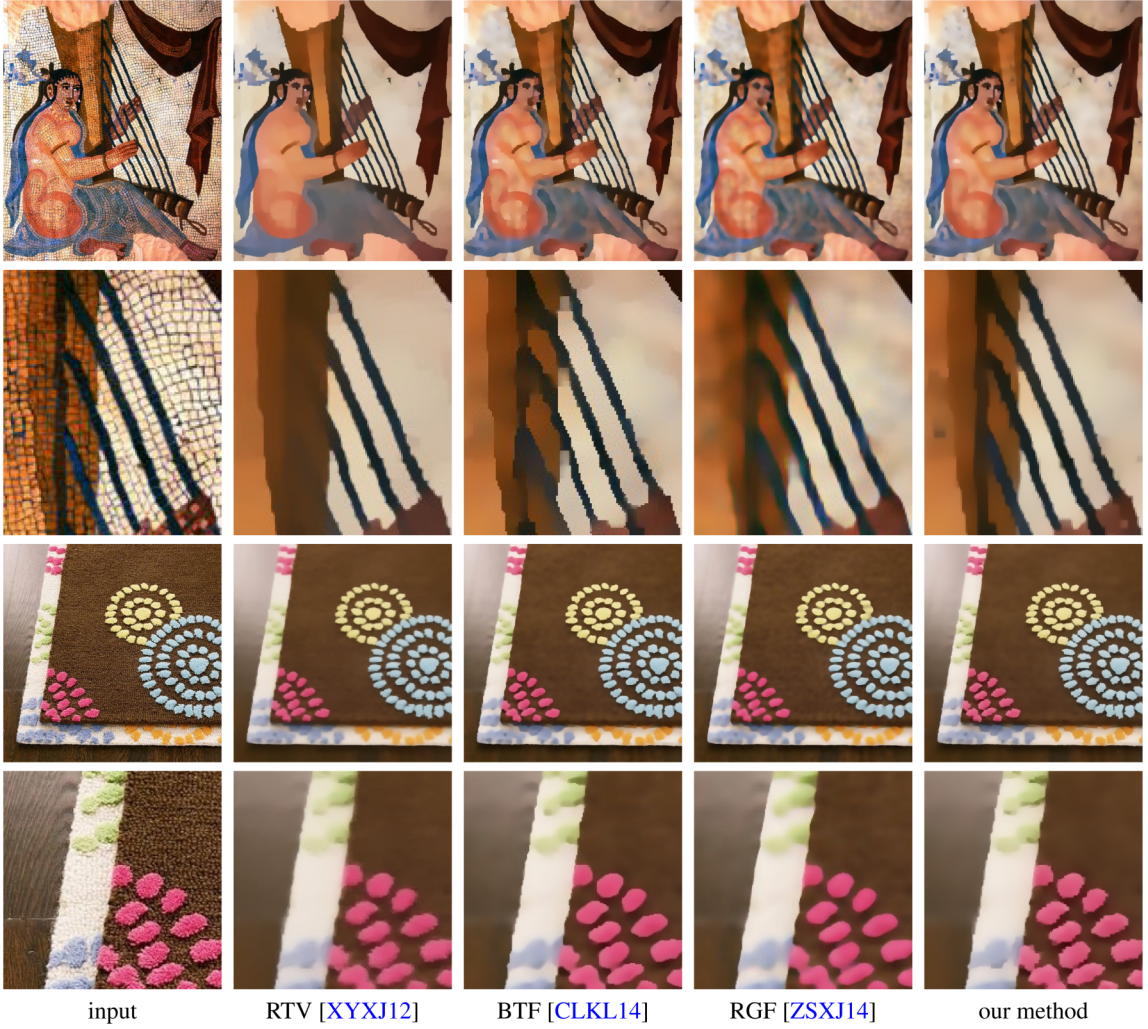


Figure 10: Comparison of filtering results. Input images contain strong textures as well as sharp edges and smoothly varying shadings. As compared to other methods, our method removes textures while preserving image structures and shading better.

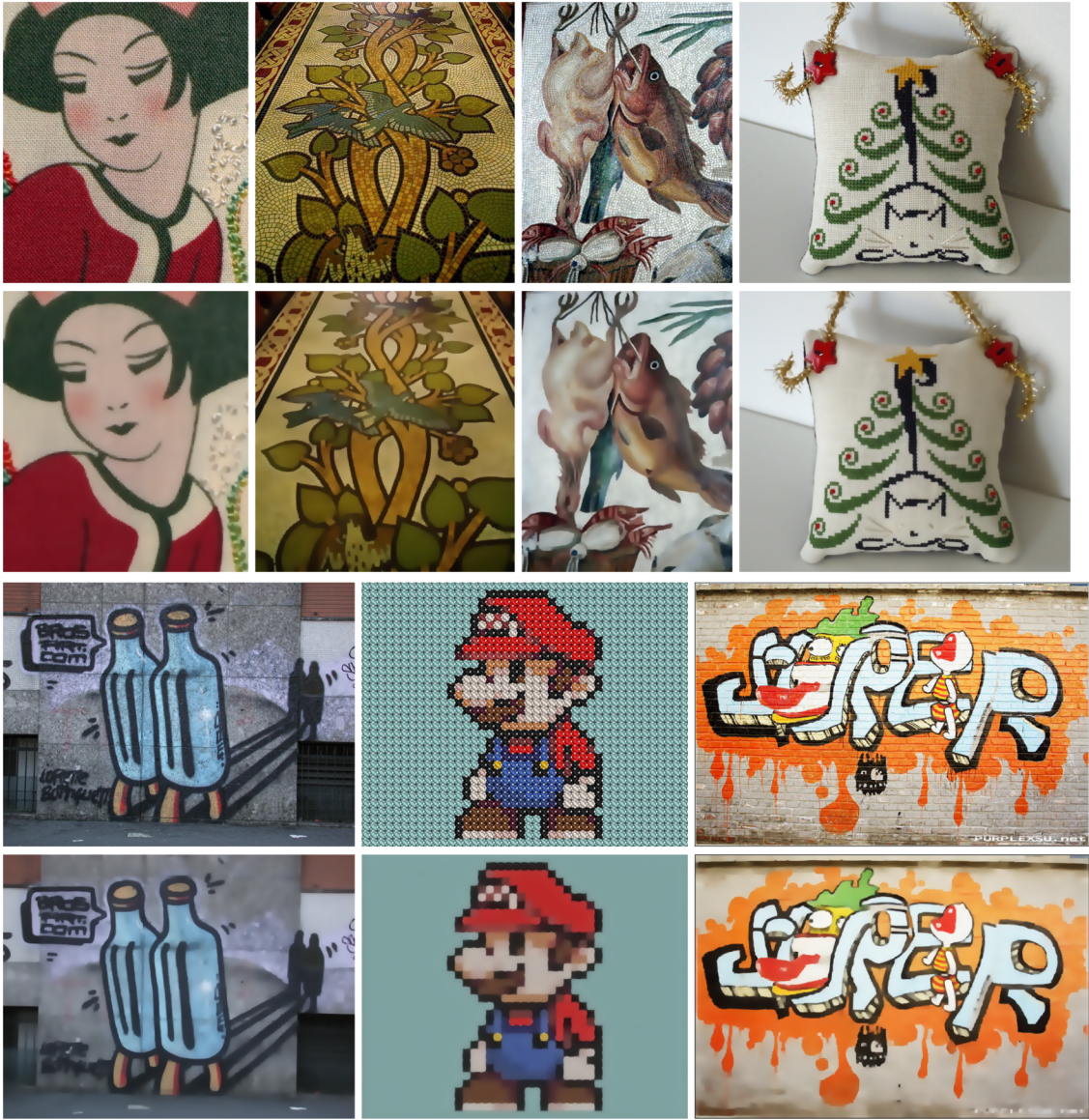


Figure 11: Additional results of our structure-texture decomposition: (top) input images; (bottom) filtering results. The original gradients of structure edges in the input images are preserved well by our method, and it may make some structure edges appear a little blurry in the filtering results.

appear sharper and cleaner. In contrast, our method preserves overall shading of images and retains important structure edge gradients. Additional filtering results of our method are shown in Figure 11 and the supplementary material. Note that the original gradients of the structure edges in the input images are preserved well by our method and this may cause some structure edges to appear little blurry in our filtering results.

Applications. Because of the structure-texture decomposition property, the most intuitive application of our method would be detail enhancement. In enhancing details of images, it is crucial to

precisely preserve structure edge gradients to achieve high-quality results, and this requirement prohibits many filtering-based approaches from being effectively used in detail enhancement. Our method does not distort the gradients of structure edges, even after removal of highly contrasting textures. With our method, high-quality detail enhancement results can be obtained within seconds. Figure 12 shows an example; more results can be seen in the supplementary material. As another application, Figure 13 shows an example where our method is used for inverse halftoning. Although we do not provide specific examples, our method can also be used for other applications, such as noise removal, tone mapping and texture replacement.

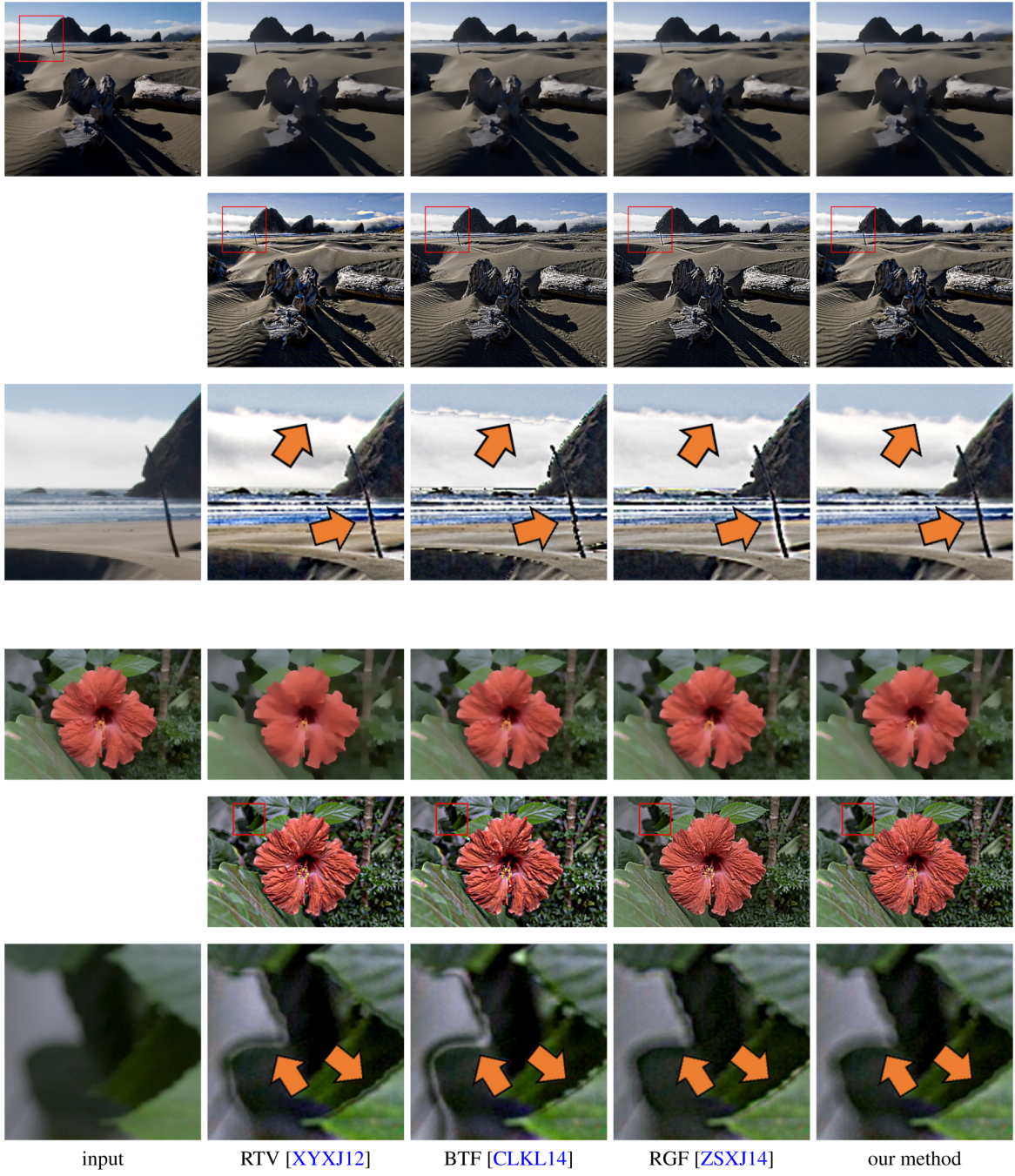


Figure 12: Comparison of detail enhancement results: (top) input and texture-filtered results; (middle) detail enhancement results; (bottom) close-ups of detail enhanced images. Our method suffers less from gradient reversal artefacts such as halos and noise. Parameters: (top example) [XYXJ12] ($\lambda = 0.01, \sigma = 3$), [CLKL14] ($k = 2, n_{iter} = 2$), [ZSXJ14] ($\sigma_s = 3, \sigma_r = 0.1, n_{iter} = 5$), and our method ($\sigma = 2.5, \epsilon = 0.015^2$); (bottom example) [XYXJ12] ($\lambda = 0.01, \sigma = 3$), [CLKL14] ($k = 3, n_{iter} = 2$), [ZSXJ14] ($\sigma_s = 4, \sigma_r = 0.1, n_{iter} = 5$), and our method ($\sigma = 2.5, \epsilon = 0.02^2$).

6. Conclusion

We proposed a novel filtering-based structure-texture decomposition method. Rather than directly filtering image colours, our method

manipulates image gradients to produce high-quality filtering results with fewer artefacts than previous filtering-based approaches. We proposed a novel gradient operator, the *interval gradient*, which is a useful tool for effectively distinguishing the textures from the



Figure 13: Inverse halftoning example. Our method can effectively remove halftoning artefacts from the input image, while preserving shading and strong edges.

structures of an image. With our interval gradient operator and gradient guided image filtering, we obtained state-of-the-art structure-texture decomposition results, which can be utilized in various applications.

Limitations. Similarly to previous approaches, our method requires fixed scale parameters and cannot handle textures with largely varying scales (Figure 14a). As a local 1D filtering approach, our method cannot easily handle strong and irregular texture patterns. Since such textures can be considered as unique structures in local windows, sparse patterns may not be filtered (Figure 14b). Our method attempts to preserve 1D increasing or decreasing signals as far as possible, and filtering may not be accurate around some complex texture boundaries (Figure 14c). Lastly, our definition of the texture does not consider semantic information of the scene, and sometimes filtering results could be perceived non-intuitive in terms of the semantic information (Figure 14d).

Future work. Our possible future work would be to address these limitations. Ham *et al.* [HCP15] recently proposed a novel optimization-based filtering method that can handle different scales of textures in the input image. It would also be interesting to find interactive applications based on our structure-texture decomposition method.

Acknowledgements

This work was supported by Institute for Information & Communications Technology Promotion (IITP) grant (R0126-16-1078) and the National Research Foundation of Korea (NRF) grant (NRF-2014R1A2A1A11052779, NRF-2013R1A1A2010619, 2015R1A5A7037615) both funded by the Korea government (MSIP, MOE).

Appendix

Interval gradient kernel in gradient domain

Let $\{I_1, I_2, \dots, I_{2n}\}$ be 1D signal values and $\{g_2, g_3, \dots, g_{2n-1}\}$ be their gradients, such that $g_i = I_{i+1} - I_i$. Then, for each pair of pixels I_p and I_q where $p < q$, we can express I_q as

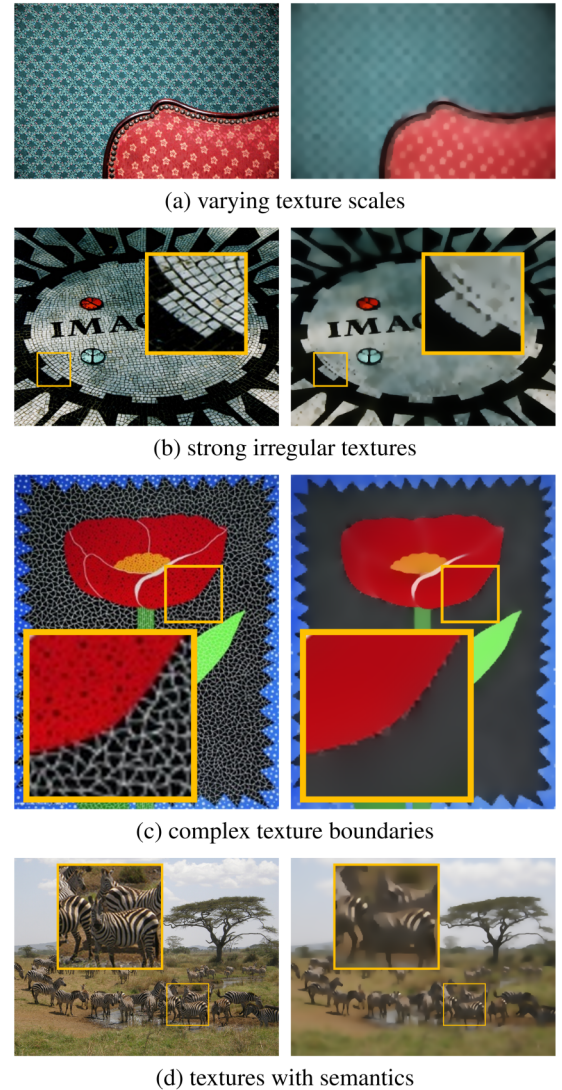


Figure 14: Limitation cases: (a) our method cannot easily handle textures with largely varying scales; (b) some strong, irregular textures may not be filtered since they can be considered as structures in local windows; (c) our method attempts to preserve monotonic signals in 1D, causing some complex texture boundaries are not accurately filtered; (d) our texture metric does not consider high-level semantic information, and some stripe patterns of zebras have not been smoothed.

$$I_q = I_p + \sum_{k=p}^{q-1} g_k. \quad (\text{A.1})$$

With a symmetric interval gradient kernel, the interval gradient of the n -th pixel is computed as

$$\nabla_\Omega I_n = \sum_{k=n+1}^{2n} w_k I_k - \sum_{k=1}^n w_k I_k, \quad (\text{A.2})$$

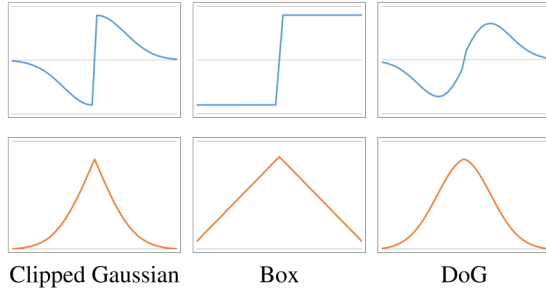


Figure 15: (Top) interval gradient kernels in the intensity domain; (bottom) corresponding equivalents in the gradient domain. For the kernels in the bottom row, the area under the curve is greater than 1 (not normalized) and their maximum values are always 1.

where w represents symmetric kernel weights such that $w_{2n-k} = w_k$ for $k \in \{1, \dots, n\}$.

Equation (A.2) can be rearranged as

$$\nabla_\Omega I_n = \sum_{k=1}^n w_k (I_{2n-k+1} - I_k), \quad (\text{A.3})$$

and by substituting I_{2n-k+1} using Equation (A.1) we obtain

$$\nabla_\Omega I_n = \sum_{k=1}^n w_k \sum_{i=k}^{2n-k} g_i. \quad (\text{A.4})$$

By rearranging in terms of g , we obtain

$$\nabla_\Omega I_n = \sum_{k=1}^{2n-1} \bar{w}_k g_k, \quad (\text{A.5})$$

where \bar{w} represents the symmetric weights with length of $2n - 1$, such that

$$\bar{w}_k = \begin{cases} \sum_{i=1}^k w_k & k \in \{1, \dots, n\} \\ \sum_{i=1}^{2n-k} w_k & k \in \{n + 1, \dots, 2n - 1\} \end{cases}, \quad (\text{A.6})$$

which becomes unnormalized smoothing of gradients. Figure 15 shows interval gradient kernels and their corresponding smoothing kernels in the gradient domain.

Power spectrum analysis

Figure A1 shows an example of the power spectrum analysis. Gaussian smoothing blurs not only textures but also structure edges, causing most high-frequency energies suppressed and flattened in the power spectrum. Our filtering method, on the other hand, smoothes high-frequency textures but preserves sharp structure edges, resulting in the power spectrum where high-frequency energies have been reduced overall but still remain due to some from sharp structure edges. Figure A1(d) shows that the power spectrum of the filter-

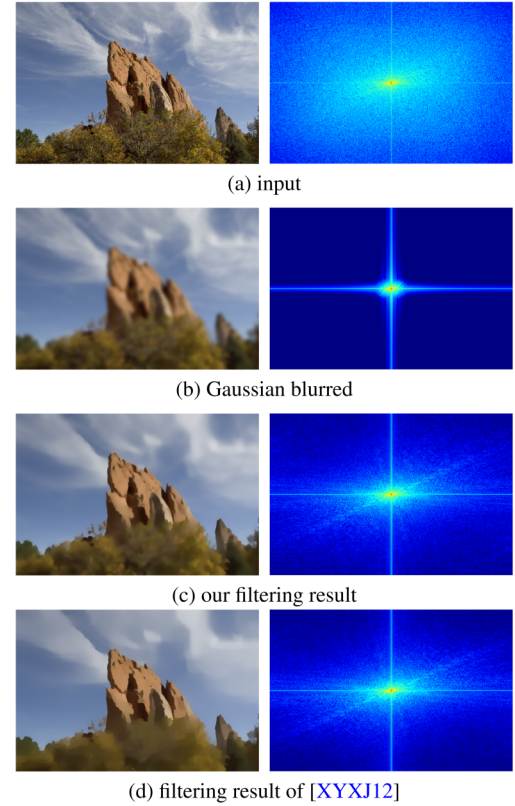


Figure A1: Power spectrum analysis example: (left) input and smoothed images; (right) power spectrums of the images. Best viewed on a colour screen.

ing result of the state-of-the-art optimization-based texture-filtering method [XYXJ12] is quite similar to ours.

References

- [Aga07] AGARWALA A.: Efficient gradient-domain compositing using quadtrees. *ACM Transactions on Graphics* 26, 3 (2007), Article No. 94.
- [AR07] AGRAWAL A., RASKAR R.: Gradient domain manipulation techniques in vision and graphics. In *Proceedings of ICCV 2007* (Tutorials, Rio de Janeiro, Brazil, 2007).
- [BFGS03] BOLZ J., FARMER I., GRINSPUN E., SCHRÖDER P.: Sparse matrix solvers on the GPU: Conjugate gradients and multigrid. *ACM Trans. Graphics (Proc. SIGGRAPH 2003)* 22, 3 (2003), 917–924.
- [BST*14] BONNEEL N., SUNKAVALLI K., TOMPKIN J., SUN D., PARIS S., PFISTER H.: Interactive intrinsic video editing. *ACM Transactions on Graphics (Proceedings of SIGGRAPH 2014)* 33, 6 (2014), Article No. 197.
- [BZCC10] BHAT P., ZITNICK C. L., COHEN M., CURLESS B.: Gradientshop: A gradient-domain optimization framework for image

- and video filtering. *ACM Transactions on Graphics* 29, 2 (2010), Article No. 10.
- [CLKL14] CHO H., LEE H., KANG H., LEE S.: Bilateral texture filtering. *ACM Transactions on Graphics* 33, 4 (2014), Article No. 128.
- [FFLS08] FARBMAN Z., FATTAL R., LISCHINSKI D., SZELISKI R.: Edge-preserving decompositions for multi-scale tone and detail manipulation. *ACM Transactions on Graphics* 27, 3 (2008), 67:1–67:10.
- [FHL*09] FARBMAN Z., HOFFER G., LIPMAN Y., COHEN-OR D., LISCHINSKI D.: Coordinates for instant image cloning. *ACM Transactions on Graphics* 28, 3 (2009), Article No. 67.
- [FLW02] FATTAL R., LISCHINSKI D., WERMAN M.: Gradient domain high dynamic range compression. *ACM Transactions on Graphics* 21, 3 (2002), 249–256.
- [GJAF09] GROSSE R., JOHNSON M. K., ADELSON E. H., FREEMAN W. T.: Ground truth dataset and baseline evaluations for intrinsic image algorithms. In *Proceedings of ICCV 2009*, (Kyoto, Japan, 2009), IEEE, pp. 2335–2342.
- [GO11] GASTAL E. S. L., OLIVEIRA M. M.: Domain transform for edge-aware image and video processing. *ACM Transactions on Graphics* 30 (2011), 69:1–69:12.
- [GWL*03] GOODNIGHT N., WOOLLEY C., LEWIN G., LUEBKE D., HUMPHREYS G.: A multigrid solver for boundary value problems using programmable graphics hardware. In *Proceedings of Graphics Hardware* (Aire-la-Ville, Switzerland, Switzerland, 2003), Eurographics Association, pp. 102–111.
- [HBZW14] HUA M., BIE X., ZHANG M., WANG W.: Edge-aware gradient domain optimization framework for image filtering by local propagation. In *Proceedings of CVPR*, (Columbus, OH, 2014), IEEE, pp. 2838–2845.
- [HCP15] HAM B., CHO M., PONCE J.: Robust image filtering using joint static and dynamic guidance. In *Proceedings of CVPR*, (Boston, MA, 2015), IEEE, pp. 4823–4831.
- [HST10] HE K., SUN J., TANG X.: Guided image filtering. *pami* 35, 6 (2010), 1397–1409.
- [KEE13] KARACAN L., ERDEM E., ERDEM A.: Structure-preserving image smoothing via region covariances. *ACM Transactions on Graphics* 32, 6 (2013), 176:1–176:11.
- [KS10] KASS M., SOLOMON J.: Smoothed local histogram filters. *ACM Transactions on Graphics* 29, 4 (2010), 100:1–100:10.
- [LM71] LAND E. H., McCANN J. J.: Lightness and retinex theory. *Journal of the Optical Society of America* 61, 1 (1971), 1–11.
- [MCL*14] MIN D., CHOI S., LU J., HAM B., SOHN K., DO M. N.: Fast global image smoothing based on weighted least squares. *IEEE Transactions on Image Processing* 23, 12 (2014), 5638–5653.
- [MHW*13] MA Z., HE K., WEI Y., SUN J., WU E.: Constant time weighted median filtering for stereo matching and beyond. In *Proceedings of ICCV 2013*, (Sydney, NSW, 2013), IEEE, pp. 49–56.
- [NBGS08] NICKOLLS J., BUCK I., GARLAND M., SKADRON K.: Scalable parallel programming with cuda. *Queue* 6, 2 (2008), 40–53.
- [PGB03] PÉREZ P., GANGNET M., BLAKE A.: Poisson image editing. *ACM Transactions on Graphics* 22, 3 (2003), 313–318.
- [PHK11] PARIS S., HASINOFF S. W., KAUTZ J.: Local Laplacian filters: Edge-aware image processing with a Laplacian pyramid. *ACM Transactions on Graphics* 30, 4 (2011), 68:1–68:12.
- [ROF92] RUDIN L. I., OSHER S., FATEMI E.: Nonlinear total variation based noise removal algorithms. *Physica D* 60 (1992), 259–268.
- [SSD09] SUBR K., SOLER C., DURAND F.: Edge-preserving multi-scale image decomposition based on local extrema. *ACM Transactions on Graphics (Proceedings of SIGGRAPH Asia 2009)* 28, 5 (2009), Article No. 147.
- [TFA05] TAPPEN M. F., FREEMAN W. T., ADELSON E. H.: Recovering intrinsic images from a single image. *IEEE Transactions on Pattern Analysis Machine Intelligence* 27, 9 (2005), 1459–1472.
- [TM98] TOMASI C., MANDUCHI R.: Bilateral filtering for gray and color images. In *Proceedings of ICCV 1998*, (Bombay, India, 1998), IEEE, pp. 839–846.
- [VPS03] VANHAMEL I., PRATIKAKIS I., SAHLI H.: Multiscale gradient watersheds of color images. *IEEE Transactions on Image Processing* 12, 6 (2003), 617–626.
- [Wei98] WEICKERT J.: *Anisotropic Diffusion in Image Processing*, Vol. 1. Teubner-Verlag, Stuttgart, Germany, 1998.
- [Wei06] WEISS B.: Fast median and bilateral filtering. *ACM Transactions on Graphics* 25, 3 (2006), 519–526.
- [XLXJ11] XU L., LU C., XU Y., JIA J.: Image smoothing via L0 gradient minimization. *ACM Transactions on Graphics* 30, 5 (2011), 174:1–174:12.
- [XYXJ12] XU L., YAN Q., XIA Y., JIA J.: Structure extraction from texture via relative total variation. *ACM Transactions on Graphics* 31, 6 (2012), 139:1–139:10.
- [ZSXJ14] ZHANG Q., SHEN X., XU L., JIA J.: Rolling guidance filter. In *Proceedings of ECCV*, Fleet D., Pajdla T., Schiele B. and Tuytelaars T. (Eds.), (Zurich, Switzerland), Springer International Publishing, Vol. 8691, (2014), pp. 815–830.
- [ZXJ14] ZHANG Q., XU L., JIA J.: 100+ times faster weighted median filter. In *Proceedings of CVPR 2014*, (Columbus, OH, 2014), IEEE, pp. 2830–2837.

Supporting Information

Additional Supporting Information may be found in the online version of this article at the publisher's web site:

Data S1